

## Research Article

# Zero-Offset VSP Monitoring of CO<sub>2</sub> Storage: Impedance Inversion and Wedge Modelling at the Ketzin Pilot Site

Julia Götz,<sup>1</sup> Stefan Lüth,<sup>1</sup> Charlotte M. Krawczyk,<sup>2,3</sup> and Calin Cosma<sup>4</sup>

<sup>1</sup>GFZ German Research Centre for Geosciences, Telegrafenberg, 14473 Potsdam, Germany

<sup>2</sup>Leibniz Institute for Applied Geophysics (LIAG), Stilleweg 2, 30655 Hannover, Germany

<sup>3</sup>TU Berlin, Fachgebiet Angewandte Geophysik, Institut für Angewandte Geowissenschaften, Sekr. BH 1-1, Ernst-Reuter-Platz 1, D-10587 Berlin, Germany

<sup>4</sup>Vibrometric Oy, Taipaleentie 127, 01860 Perttula, Finland

Correspondence should be addressed to Julia Götz; [jgoetz@gfz-potsdam.de](mailto:jgoetz@gfz-potsdam.de)

Received 28 May 2014; Revised 28 October 2014; Accepted 28 October 2014; Published 14 December 2014

Academic Editor: Joerg Schleicher

Copyright © 2014 Julia Götz et al. This is an open access article distributed under the Creative Commons Attribution License, which permits unrestricted use, distribution, and reproduction in any medium, provided the original work is properly cited.

At the CO<sub>2</sub> storage pilot site near the town of Ketzin (35 km west of Berlin, Germany) the sandstone reservoir at 630 m–650 m depth is thin and heterogeneous. The time-lapse analysis of zero-offset VSP measurements shows that CO<sub>2</sub>-induced amplitude changes can be observed on near-well corridor stacks. Further, we investigate whether CO<sub>2</sub>-induced amplitude changes in the monitoring data can be used to derive geometrical and petrophysical parameters governing the migration of CO<sub>2</sub> within a brine saturated sandstone aquifer. 2D seismic-elastic modelling is done to test the processing workflow and to perform a wedge modelling study for estimation of the vertical expansion of the CO<sub>2</sub> plume. When using the NRMS error as a measure for the similarity between the modelled and recorded repeat traces, the best match is achieved for a plume thickness of 6–7 m within the reservoir sandstone of 8 m thickness. With band limited impedance inversion a velocity reduction at the top of the reservoir of 30%, influenced by casing reverberations as well as CO<sub>2</sub> injection, is found. The relation of seismic amplitude to CO<sub>2</sub> saturated layer thickness and CO<sub>2</sub>-induced changes in P-wave velocities are important parameters for the quantification of the injected CO<sub>2</sub> volume.

## 1. Introduction

The geological storage of CO<sub>2</sub>, as last step of the carbon capture and storage (CCS) process chain, is applied and investigated in several pilot and demonstration projects at different scales, for example, in Cranfield (USA [1]), Frio (USA [2]), In Salah (Algeria [3]), Ketzin (Germany [4]), Nagaoka (Japan [5]), Otway (Australia [6]), Sleipner (Norway [7]), and Weyburn (Canada [8]). Among these, deep saline aquifers are the geological structures which have the largest storage potential worldwide [9]. To study the behaviour of a reservoir during injection and stabilisation, seismic time-lapse investigations at different scales were established. Seismic monitoring of the spreading of CO<sub>2</sub> in a saline aquifer is based on the following time-lapse effects: as CO<sub>2</sub> replaces saline water, the impedance contrast between the gas filled reservoir and the caprock is increased, which leads to stronger

reflections from top of the reservoir. Furthermore, due to the reduced velocities in the gas filled reservoir, time delays of reflections from underneath can be observed.

The 2D and 3D surface seismic methods [10–12] generally are accompanied by high-resolution methods like crosshole seismic [13, 14] or Vertical Seismic Profiling (VSP, [15]). A VSP survey, monitoring a small scale CO<sub>2</sub> injection in a brine aquifer of the Frio Formation, is described by Daley et al. [16]. They find a large (~70%) increase in reflection amplitude for the Frio horizon and compared the VSP results with numerical modelling. A good qualitative agreement of the plume extent is found. Azimuthal differences in the reflection amplitudes are attributed to lateral heterogeneities imaged by the VSP which are not captured in the model.

At the CO<sub>2</sub> storage site near the town Ketzin in Germany, within 5 years of operation, between June 2008 and August 2013, 67 kt of food-grade CO<sub>2</sub> has been injected into a saline

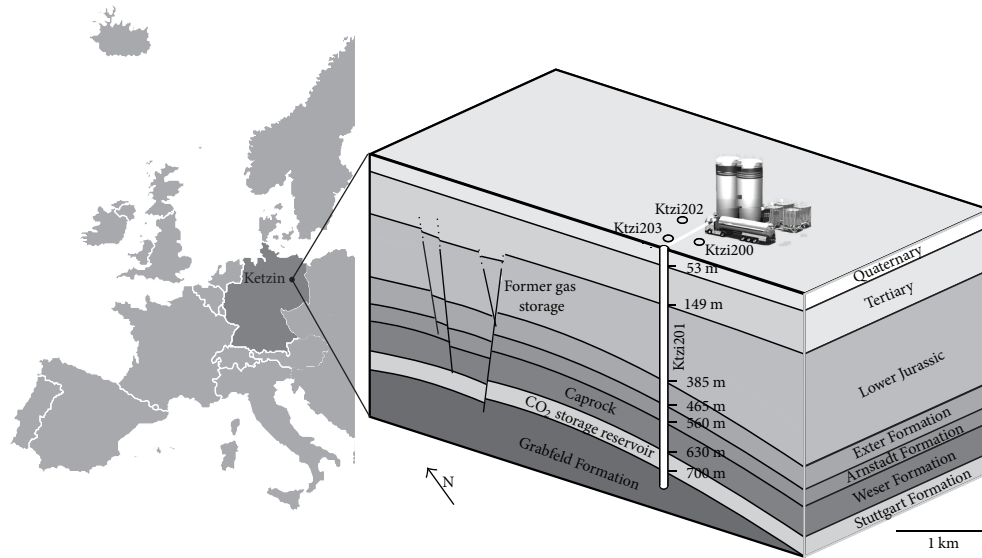


FIGURE 1: Location and structure of the Ketzin storage site. Left: Ketzin is located in the Federal State of Brandenburg (Germany) about 35 km west of Berlin. The Ketzin site is marked as a dot. Right: schematic and vertically exaggerated block diagram of the Ketzin storage site (not to scale, modified after Liebscher et al. [27]) illustrating the structure and stratigraphy of the Ketzin anticline. The target CO<sub>2</sub> storage zone in the upper part of the Stuttgart Formation covers the range of 630 m–650 m below ground level.

sandstone reservoir [4]. The storage site is part of an anticlinal structure in the northeast German Basin (Figure 1, [17, 18]). The sandstone reservoir is located at a depth of 630 m–650 m below the injection site in the upper part of the Triassic Stuttgart Formation.

An important part of the scientific program at Ketzin is the site characterisation and the monitoring of the subsurface migration of CO<sub>2</sub> with several seismic methods at different scales, ranging from 3D surface seismic to laboratory measurements. One of the key results of the 3D surface seismic monitoring is a map of the lateral distribution of CO<sub>2</sub> in the reservoir [19]. Figure 2 shows the normalised amplitude difference (repeat minus baseline) at the reservoir horizon (top of Stuttgart Formation). The amplitude difference is the result of time-lapse processing of the baseline and repeat surveys, which were recorded in autumn 2005 and in autumn 2009, respectively. At the time of the repeat survey 22 kt–25 kt have been injected (Table 1). The CO<sub>2</sub> is visible in the difference map as strong amplitudes at the time interval of the reservoir.

In addition, the effect of supercritical CO<sub>2</sub> injection on the P-wave and S-wave velocities of the Ketzin reservoir is investigated at laboratory scale [20]. The experiments were carried out on two sandstone core samples from the Stuttgart Formation. The measurements demonstrated that CO<sub>2</sub> injection has hardly an effect on the S-wave velocity. The influence of CO<sub>2</sub> saturation on the P-wave velocity is different for both samples. For the first sample, the maximum measurable CO<sub>2</sub> saturation was 50%–60%, associated with a P-wave velocity reduction of 15%–16%. For the second sample, the maximum measurable CO<sub>2</sub> saturation was 40%, associated with a P-wave velocity reduction of 20%–21%. These results reflect the heterogeneity of the reservoir sandstone [21].

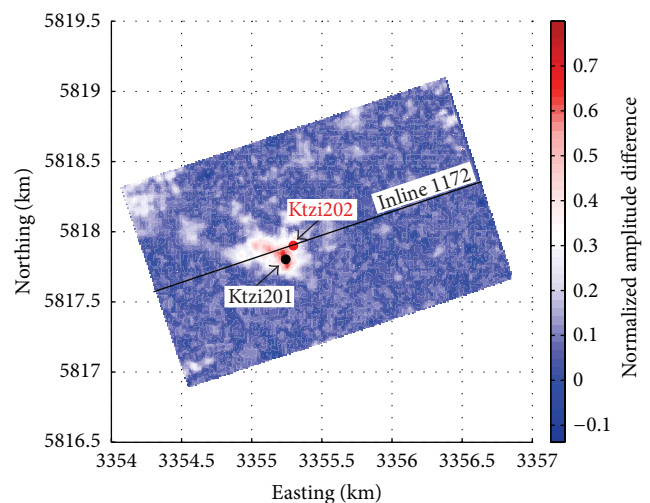


FIGURE 2: Map of the normalised amplitude difference (repeat minus baseline) at the reservoir horizon (top of Stuttgart Formation). The difference is the result of time-lapse processing of the 3D surface seismic baseline (recorded autumn 2005) and repeat surveys (recorded autumn 2009 [19]). The injection well Ktzi201 and the observation well Ktzi202 are marked as dots. The inline 1172, which is crossing the observation well Ktzi202, is indicated by the black line.

The surface seismic measurements in Ketzin are accompanied by several surface-to-borehole seismic methods like Moving Source Profiling (MSP, [22]) or offset and zero-offset Vertical Seismic Profiling (VSP). Borehole seismic methods are expected to have a higher resolution than surface seismic methods. The zero-offset VSP was acquired to provide near-well corridor stacks and information about normal incidence

TABLE 1: Timeline of 3D surface seismic and zero-offset VSP measurements in Ketzin with correspondent tons of CO<sub>2</sub> injected.

| Event                          | Run        | Date                          | Injected CO <sub>2</sub> |
|--------------------------------|------------|-------------------------------|--------------------------|
| 3D surface seismic             | Baseline   | Autumn 2005                   |                          |
| Zero-offset VSP                | Baseline   | November/December 2007        |                          |
| <i>Start of injection</i>      |            | 30 June 2008                  |                          |
| <i>Breakthrough in Ktzi202</i> |            | 20 March 2009, after 263 days | 11 kt                    |
| 3D surface seismic             | 1st repeat | Autumn 2009                   | 22 kt–25 kt              |
| Zero-offset VSP                | 1st repeat | February 2011                 | 46 kt                    |
| 3D surface seismic             | 2nd repeat | Autumn 2012                   | 61 kt                    |

reflectivity. We investigate whether CO<sub>2</sub>-induced amplitude changes in the zero-offset VSP monitoring data can be used to derive geometrical and petrophysical parameters governing the migration of CO<sub>2</sub> within the sandstone aquifer.

The repeatability is crucial for a successful interpretation of time-lapse data. Within the zero-offset VSP data, time-lapse differences which are not related to CO<sub>2</sub> injection are caused by the usage of slightly different seismic sources (Section 2.1) and by an unfavourable casing situation giving rise to casing reverberations (Section 2.2). To compensate for these effects, the standard VSP processing (Section 2.3) is followed by time-lapse processing (Section 2.4). Based on the time-lapse processed data a band limited impedance inversion (method after Ferguson and Margrave [23]) is performed to calculate the reduction of P-wave velocity due to CO<sub>2</sub> injection (Section 4). In order to verify the quality of the inversion, it is also applied to modelled time-lapse data (Section 3) with the aim to recover the velocity contrast between the baseline and repeat velocity models. Furthermore, the 2D seismic-elastic modelling is done to test the processing workflow and to perform a wedge modelling study in order to estimate the vertical expansion of the CO<sub>2</sub> plume below the top of the reservoir (Section 5.3).

Based on a petrophysical model, changes in P-wave velocities can be related to the CO<sub>2</sub> saturation. The vertical expansion of the CO<sub>2</sub> plume and the saturation are important parameters for the quantification of the injected CO<sub>2</sub> volume.

## 2. Acquisition and Processing

**2.1. Acquisition.** Prior to injection the zero-offset VSP baseline was recorded in November/December 2007; the repeat survey was conducted in February 2011 with ~46 kt of CO<sub>2</sub> injected (Table 1). The location of the injection well “CO<sub>2</sub> Ktzi 201/2007” (Ktzi201) is 112 m apart from the observation well “CO<sub>2</sub> Ktzi 202/2007” (Ktzi202), where the zero-offset VSPs were recorded (Figure 2).

The source and receiver layouts of the zero-offset VSP baseline and repeat measurements are listed in Table 2. The baseline was recorded at 132 depth levels, from 45 m to 700 m below ground level. The vertical distance between the levels is 5 m. The source was activated on asphalt within the range of a few meters to the observation well Ktzi202. Since the upper part of the baseline wavefield is affected by strong casing waves (Figure 3, [24, 25]), the repeat measurement has

TABLE 2: Summary of source and receiver layout for the zero-offset VSP baseline and repeat measurements. The number of depth levels and the depth range used for processing and imaging are listed as well. The depth is in meter below ground level (m b.gl.).

| Measurement/dataset  | Number of depth levels | Depth range                    | Source   |
|----------------------|------------------------|--------------------------------|--|
| Baseline             | 132                    | 45–700 m b.gl.<br>5 m spacing  | 5 m distance to well<br>activated on asphalt<br>VIBSIST-1000 |
| Repeat               | 80                     | 325–720 m b.gl.<br>5 m spacing | 10 m distance to well<br>activated on gravel<br>VIBSIST-3000 |
| Processed and imaged | 49                     | 460–700 m b.gl.<br>5 m spacing |  |

been modified. The influence of the casing is sought to be reduced by moving the source a few meters and activating it on gravel. Furthermore, only the lower part of the zero-offset VSP was repeated. The repeat was recorded at 80 depth levels, from 325 m to 720 m below ground level (m b.gl.). The vertical component of the data sets and only data which are not affected by casing waves (460 m–700 m b.gl., 49 depth levels) are used for further processing and imaging.

As for the 2D surface seismic and Moving Source Profiling in Ketzin [22], a VIBSIST source was used for the zero-offset VSP measurements (Swept Impact Seismic Technique, SIST, [26]). For the repeat survey a further development of the VIBSIST was used, for which the hammer impact energy has been enhanced from 2500 J/impact to 3000 J/impact. The data recording was conducted with 3-component RD-XYZ-cg receivers [22]. After the breakthrough of CO<sub>2</sub> in the observation well Ktzi202 (Figure 2, Table 1), a lubricator is needed to access the pressurised well with the receiver string during the repeat measurement. The sample rate of the recorded traces is 0.25 ms; the recording lengths are 2499.75 ms and 2047.75 ms for the baseline and repeat surveys, respectively.

The usage of slightly different source types at different locations and surfaces decreases the repeatability and makes time-lapse processing necessary.

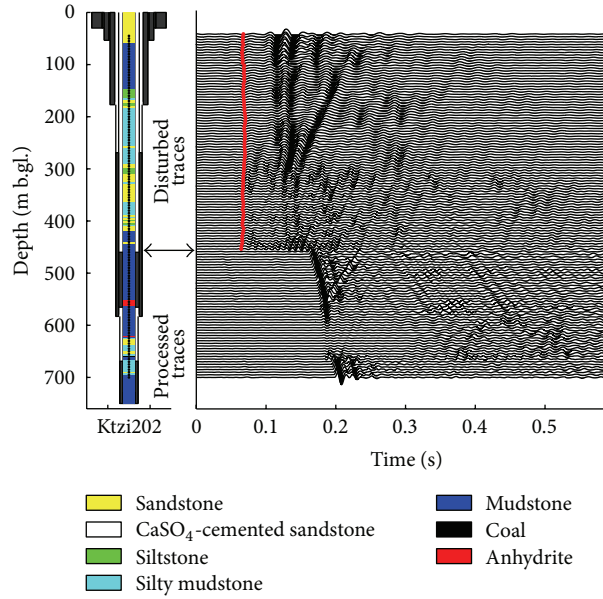


FIGURE 3: Vertical component of the baseline zero-offset VSP together with the casing of Ktzi202 and the lithology within the well (modified after Daley et al. [25]). Left: casing and cementation (grey) of Ktzi202; the lithology is plotted in the centre of the well [21]. Right: zero-offset VSP, vertical component with trace balance, and linear moveout with 6100 m/s steel velocity [28]. The first breaks in the upper part are marked with red dots.

**2.2. Influence of the Uncemented Casing on the Data.** As described in Kazemeini et al. [24], in the upper part of the survey, no clear first arrivals could be identified, because of a poorly cemented casing. Casing and cementation of Ktzi202 are shown in Figure 3 (modified after Daley et al. [25]). Large parts of the observation well are completed with multiple casings, not cemented to one another or to the formation. The casing is cemented to one another and to the formation only from 460 m to 565 m and from 669 m to 750 m depth. This is an unfavourable casing situation for recording VSP data [28], since there is no solid medium (cement) between the casing and the formation to transmit the seismic energy. The vertical component of the baseline zero-offset VSP is shown on the right side of Figure 3. The traces are balanced and a linear moveout with steel velocity (6100 m/s, [25]) was applied. Apparently, the waves down to 460 m below ground level (m b.g.l.) travel along the uncemented steel casing (casing waves). At 460 m b.g.l., the first onsets are shifted and the identification of first breaks is possible when the receivers are placed in cemented multiple casings. The signal strength again is seriously reduced between 565 m and 670 m, but the identification of phases is still possible (uncemented single casing situation).

**2.3. Zero-Offset VSP Processing.** The zero-offset VSP data is processed, following a similar processing flow as in Kazemeini et al. [24]. The raw data of recorded and modelled zero-offset VSP are shown in Figure 4. The generation of the modelled data is described in Section 3. Following the preprocessing (shift-and-stack), the processing of the zero-offset VSP data is divided into three steps (Table 3, [29]).

TABLE 3: Summary of the processing steps applied to the zero-offset VSP data.

| Step/purpose              | Parameters  |
|---------------------------|---|
| (1) Time-lapse processing | Enhance sampling rate to 0.1 ms<br>Cross-correlation time-shift |
| (2) VSP processing        | Wavefield separation (9-point median filter)                    |
| (3) VSP processing        | Trace balance<br>Outside corridor mute (60 ms)                  |
| (4) Time-lapse processing | Bandpass filter (10–20–80–100 Hz)<br>Wiener filter              |

- (1) The repeat traces are matched to the baseline traces by application of a cross-correlation time-shift [30]. First, the sampling rate of baseline and repeat data is increased to 0.1ms to allow a finely resolved time-shift. Then, the cross-correlation of baseline and repeat traces is calculated. Finally, the time-shift between the maximum amplitude of the cross-correlation and the zero-lag is applied to the repeat data.
- (2) The wavefield separation is done with a 9-point median filter. The upgoing waves are shifted by the first break times to the two-way-time and enhanced with a 9-point median filter. The 9-point median filters, compared to filters of different order, best enhanced the upgoing waves while eliminating the downgoing waves. The horizontally aligned upgoing waves are shown in Figure 4 for the recorded and modelled data.

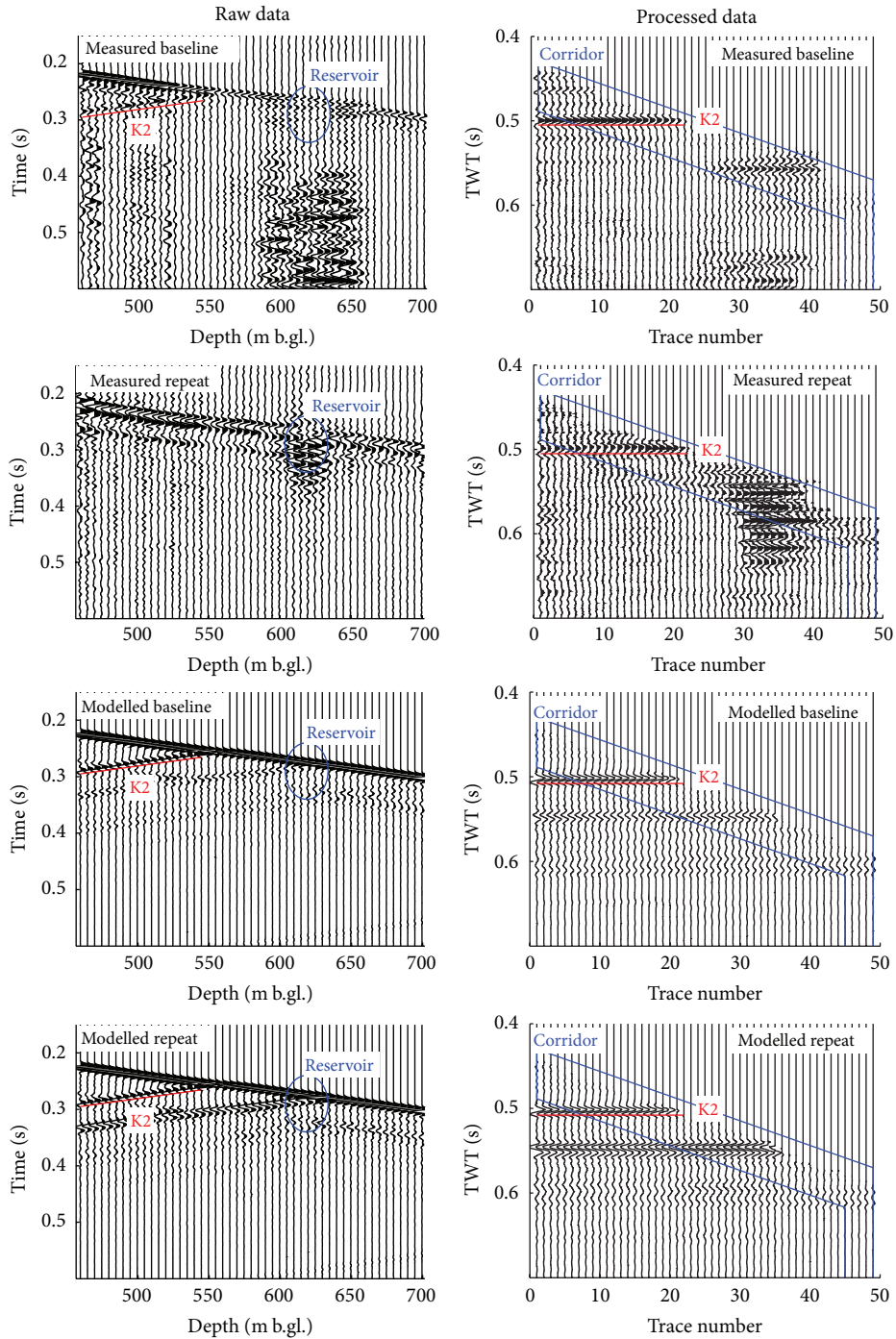


FIGURE 4: Zero-offset VSP vertical component, raw data (left column), and processed data after removal of downgoing waves, horizontal alignment, and enhancement of upgoing waves (right column). The measured baseline, measured repeat, modelled baseline, and modelled repeat data are shown from top to bottom. Reflections from an anhydrite layer (Figure 3, ~550 m below ground level), labelled K2, are marked by red lines and the depth of the reservoir is indicated by the blue circle. The blue polygons denote the corridor mute window.

(3) After trace balancing, the last step is the application of an outside corridor mute of 60 ms to account for propagation effects of upgoing waves, such as multiples [31]. The width of the corridor mute was adjusted to achieve good correlation between the zero-offset VSP data and the 3D surface seismic data.

Figure 4 shows baseline and repeat data of the zero-offset VSP after removal of downgoing waves, horizontal alignment, and enhancement of upgoing waves. A reflection from an anhydrite layer (Figure 3, ~550 m below ground level), labelled K2, is observed and marked by red lines. In the baseline data (Figure 4, top left), at the depth range

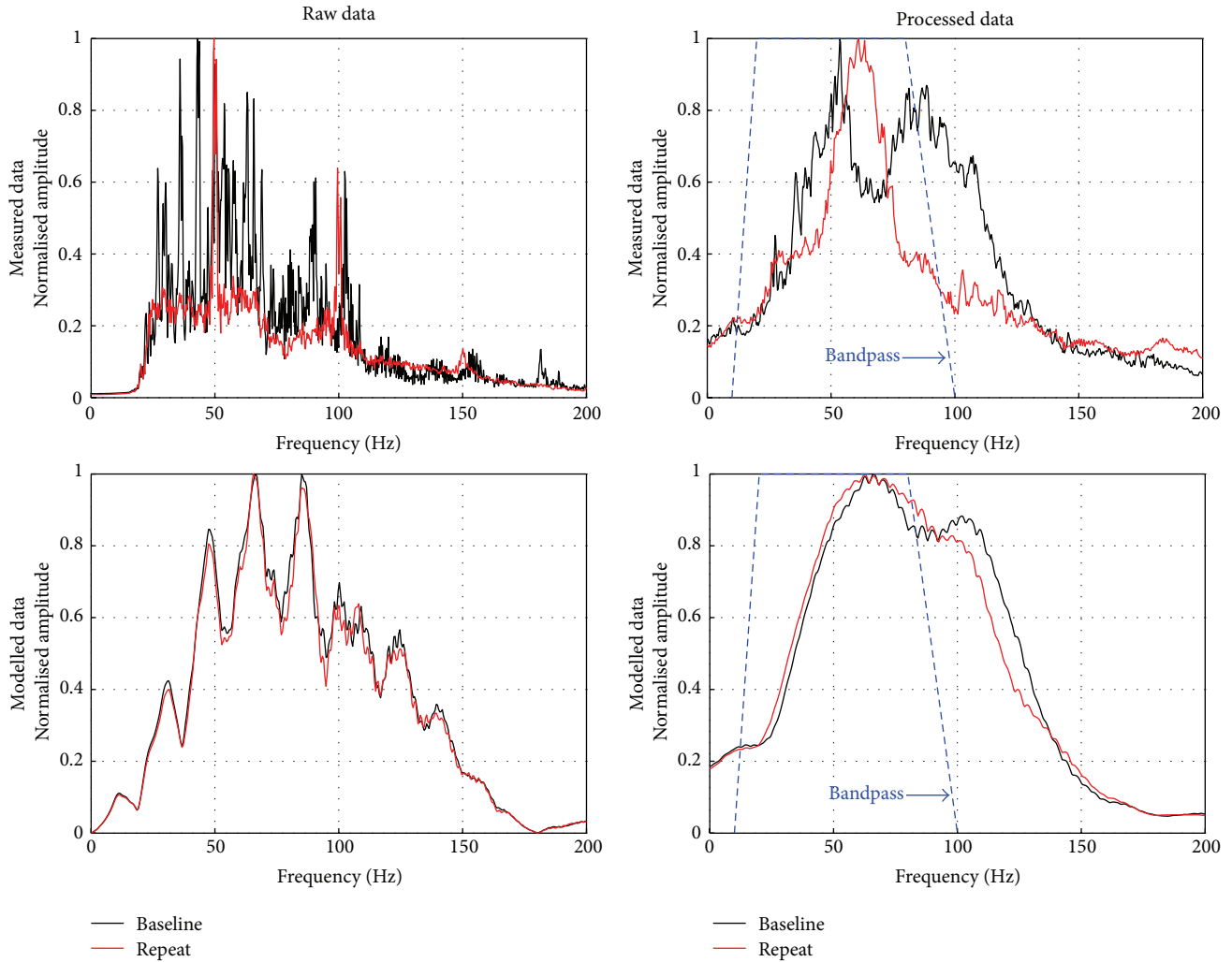


FIGURE 5: Normalised amplitude spectra of the zero-offset VSP baseline for measured and modelled data (top and bottom row). Baseline and repeat measurements are plotted as black and red lines. In the left and right columns, spectra of raw data and processed data are shown. The blue line indicates the corner frequencies of a bandpass filter (10–20–80–100 Hz) which is applied during the processing.

of the reservoir, a resonance in the wavefield from 0.65 s downward is observed. This is related to an uncemented part of the single casing string (Figure 3). The wavefield of the repeat data displays similar resonance within the reservoir after the first breaks. The differences between baseline and repeat measurements will be commented on in Section 5. Comparing the baseline (Figure 4, top row) and repeat data (Figure 4, 2nd row), one can notice the increased amplitudes at the two-way-time of the reservoir ( $\sim 0.55$  s).

**2.4. Time-Lapse Processing.** Figure 5 shows the amplitude spectra of the zero-offset VSPs for recorded and modelled data. The main frequency content lies between 25 Hz and 125 Hz, with a centre frequency of 60 Hz. There is a clear difference in the frequency spectra of baseline and repeat data (Figure 5, top right): the baseline spectrum exhibits two amplitude peaks at 50 Hz and 80 Hz, whereas the repeat spectrum has one main frequency of 60 Hz. The differences between the frequency content of baseline and repeat data

will be discussed in Section 5. In order to make the baseline and repeat measurements comparable, a bandpass filter with corner frequencies of 10–20–80–100 Hz (blue line in Figure 5) followed by a Wiener filter is applied to the baseline and repeat data [32].

### 3. Modelling of Zero-Offset VSP Data

Modelling of zero-offset VSP data is done to test the processing workflow and to perform a wedge modelling study for the estimation of the vertical expansion of the  $\text{CO}_2$  plume. Furthermore, the modelling is used to verify the quality of the band limited impedance inversion, with the aim to recover the velocity contrast between the baseline and repeat velocity models.

**3.1. Petrophysical Model Parameters.** The modelling is based on a 1D seismic-elastic model, for which the petrophysical parameters P-wave velocity, S-wave velocity, and density

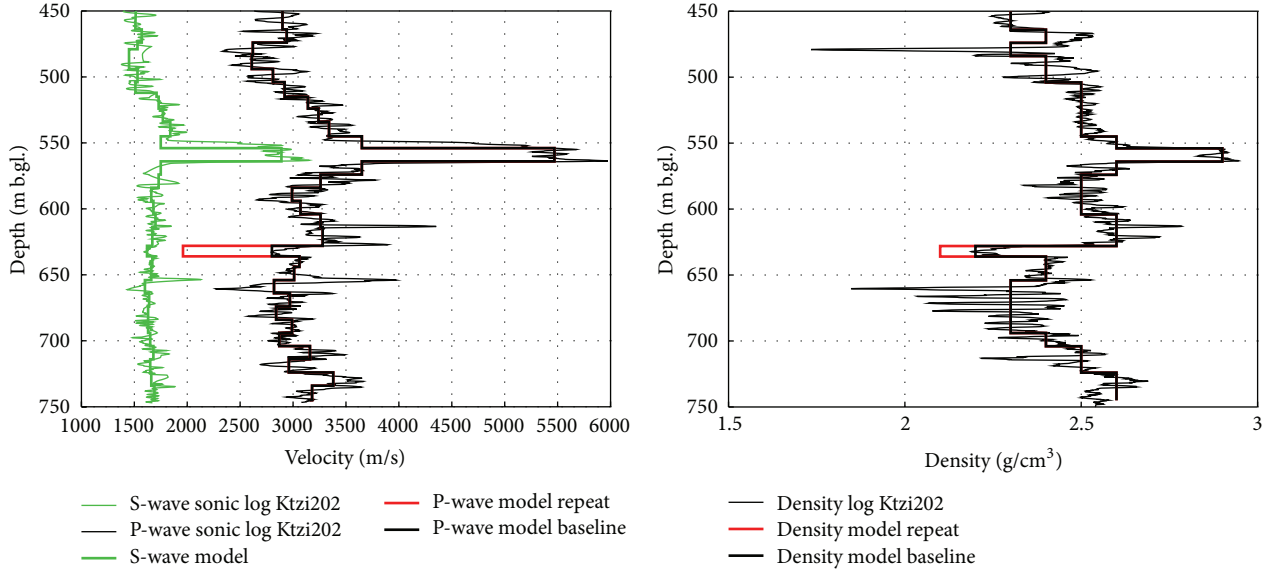


FIGURE 6: 1D seismic-elastic model based on sonic and density logs of the Ktzi202 observation well [21]. Left: P-wave and S-wave velocity model. Thin black line: P-wave sonic log of Ktzi202. Thick black line: blocky P-wave model layers. Red line: reservoir layer with a velocity reduction of 30%. Thin green line: S-wave sonic log of Ktzi202. Thick green line: blocky S-wave model layers. Right: density model. Thin black line: density log of Ktzi202. Thick black line: blocky density model layers. Red line: reservoir layer with a density reduction from  $2.2 \text{ g/cm}^3$  to  $2.1 \text{ g/cm}^3$ . The depth is in meter below ground level (m b.g.l.).

are derived from sonic and density logs of the Ktzi202 observation well [21].

The sonic and density logs are shown in Figure 6. The high velocity layer at 550 m below ground level is the anhydrite layer, which can be seen as a clear reflection (K2 reflection) in the zero-offset VSP data (Figure 4). It has the highest seismic velocities and densities:  $v_p = 5500 \text{ m/s}$ ,  $v_s = 2800 \text{ m/s}$ , and  $\rho = 2.9 \text{ g/cm}^3$ . The reservoir zone, at the depth range of 630 m–640 m, has low velocities and densities with values of  $v_p = 2800 \text{ m/s}$ ,  $v_s = 1600 \text{ m/s}$ , and  $\rho = 2.2 \text{ g/cm}^3$ .

(1) *P-Wave Velocity*. Since only zero-offset VSP receivers below 460 m below ground level are processed and imaged, a constant P-wave velocity of  $2900 \text{ m/s}$  is assumed in the upper part of the model (down to 430 m below ground level). To derive the finer structure in the lower part of the model, where the zero-offset receivers are actually placed, the P-wave sonic log of Ktzi202 (Figure 6 left, thin black line) is used to derive a blocky model with an approximate block size of 10 m (Figure 6 left, thick black line). The  $\text{CO}_2$  injection is simulated by decreasing the P-wave velocity of the model by 30% in the depth range of the reservoir (Figure 6 left, red line). This velocity reduction is chosen based on the results of the impedance inversion of the zero-offset VSP measurements (see Section 5.2).

(2) *S-Wave Velocity*. The S-wave velocity is derived in the same way and for the same model layers as the P-wave velocity (Figure 6, left). Since laboratory experiments indicated no change in S-wave velocity due to  $\text{CO}_2$  injection, the S-wave velocity is kept identical for baseline and repeat [19].

(3) *Density*. Figure 6 (right side) shows the density model, which is derived in the same way, as the P-wave velocity model, based on the density log of Ktzi202. A constant density of  $2.3 \text{ g/cm}^3$  is assumed in the upper part of the model (down to 430 m below ground level). The  $\text{CO}_2$  injection is simulated by decreasing the density from  $2.2 \text{ g/cm}^3$  to  $2.0 \text{ g/cm}^3$  within the reservoir (Figure 6 right, red line). The density reduction in the reservoir is based on the following calculations. The density of the rock matrix  $\rho_{\text{matrix}} = 2.5 \text{ g/cm}^3$  is derived with

$$\rho_{\text{brine saturated}} = \rho_{\text{matrix}} (1 - \Phi) + \rho_{\text{brine}} \Phi, \quad (1)$$

where the density of the brine saturated rock  $\rho_{\text{brine saturated}} = 2.2 \text{ g/cm}^3$  (Figure 6), the effective porosity is  $\Phi = 20\%$  [33], and the density of the brine  $\rho_{\text{brine}} = 1.2 \text{ g/cm}^3$  [19]. Based on the results of PNG logging (saturation measurements), a  $\text{CO}_2$  saturation of 50% is assumed [34]. This leads to a density of the fluid of  $\rho_{\text{fluid}} = 0.7 \text{ g/cm}^3$  calculated with

$$\rho_{\text{fluid}} = \rho_{\text{brine}} S_w + (1 - S_w) \rho_{\text{CO}_2}, \quad (2)$$

where  $S_w$  is the water saturation and  $\rho_{\text{CO}_2} = 0.2 \text{ g/cm}^3$  is the density of  $\text{CO}_2$  [19]. The density of the partially  $\text{CO}_2$  saturated rock  $\rho_{\text{CO}_2 \text{ saturated}} = 2.1 \text{ g/cm}^3$  is calculated with

$$\rho_{\text{CO}_2 \text{ saturated}} = \rho_{\text{matrix}} (1 - \Phi) + \rho_{\text{fluid}} \Phi, \quad (3)$$

where  $\rho_{\text{matrix}}$  has been calculated with (1).

3.2. *2D Finite-Difference Modelling*. The seismic wave propagation is modelled with a 2D finite-difference time-domain (FDTD) method, which does not consider attenuation and assumes the elastic parameters to be frequency independent

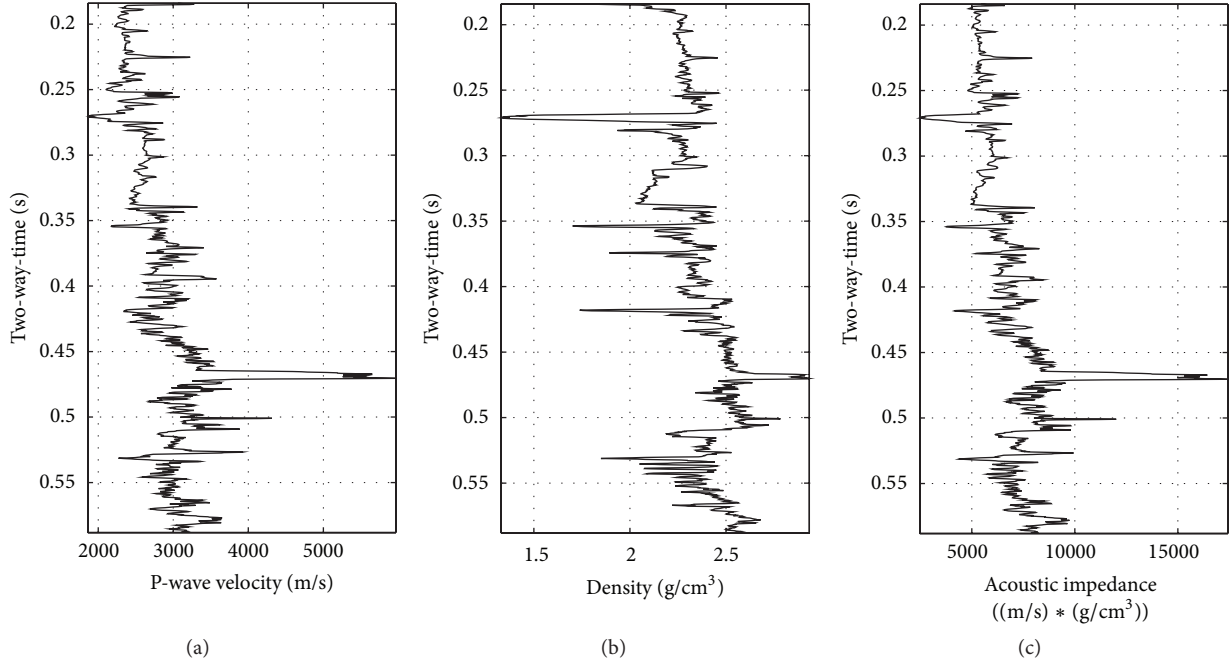


FIGURE 7: Acoustic impedance log (right) derived from the sonic and density logs (left and middle) of Ktzi202. The sonic and density logs are median filtered and converted from depth to two-way-time. Since the location of the K2 of the 3D surface seismic varies in time, the two-way-time function is shifted to the K2 for each trace. Here, as an example, the adjustment to the stacked zero-offset VSP baseline is shown (Figure 8, top left image).

[35]. The FD displacement field calculation is based on a 2nd order FD operator.

The 1D seismic-elastic model is transferred to a laterally constant 2D model. In order to avoid boundary artefacts, the boundary condition of the model is set to absorbing and the top, sides, and bottom of the model are set to distances of  $\sim 100$  m to the source and receiver locations. That leads to model dimensions of 200 m in horizontal direction and 1200 m in vertical direction. The whole model is shifted 100 m downward, leading to a thick homogeneous top layer, in which the source is located at 100 m depth. The source and receivers are placed in the centre of the model, with a horizontal offset of 10 m between source and receivers. The receivers are also shifted 100 m downward to 560 m–800 m with a vertical distance of 5 m. The source is a P-wave minimal phase, point source with a centre frequency of 60 Hz. For the FD computation the seismic-elastic model is rasterised with a given increment in horizontal and vertical direction. According to Sandmeier [35], the space increment corresponds to the minimal wave length. The critical value of the space increment for the 2D FDTD scheme is  $1/8$  of the minimum wave length ( $\lambda_{\min} = (1/8) \cdot (v_{s,\min}/f) = (1580/180)/8 \text{ m} = 1.10 \text{ m}$ , Figure 6). If this value is exceeded, numerical dispersion of the wavelet occurs. For the modelling a space increment of 1 m is chosen. The maximum time increment depends on the maximum velocity  $v_{p,\max}$  as well as on the given space increment  $\Delta x$ , with  $\Delta t \leq \Delta x / 2v_{p,\max} = 1/(2 \cdot 5500) \text{ s} = 0.09091 \text{ ms}$  (Figure 6). If  $\Delta t$  is chosen too big, the amplitude increases exponentially with time [35]. The  $\Delta t$

is set to 0.09 ms, the trace length is 2047.75 ms, equal to the real measurements, and only the vertical displacement is used for further processing and imaging.

The modelled traces are processed in the same way as the recorded traces (3rd and 4th row of Figure 4). Differences in geometrical divergence losses between 3D measurement and 2D modelling are compensated proportional to the time  $t$  for 3D losses and proportional to  $\sqrt{t}$  for 2D losses.

#### 4. Band Limited Impedance Inversion

The P-wave sonic and density logs of Ktzi202 are used to provide the low frequency content required by the inversion process [23]. The acoustic impedance log is derived from the sonic and density logs with  $z = v_p \cdot \rho$ . Figure 7 shows, from left to right, the P-wave sonic log, the density log, and the impedance log. The logs are median filtered (10-point filter) and converted from depth to two-way-time (TWT). The impedance log is tied to the 3D surface seismic by shifting the two-way-time function to the upper trough of the strong double reflection of the K2 (see Figure 8). The low and high pass frequencies for the impedance log and the seismic trace are set to 20 Hz and 90 Hz, with a Gaussian roll-off of 10 Hz. The impedances are converted to P-wave velocities with Gardner's equation [36, 37]. The result of the band limited impedance inversion of the 3D surface seismic (inline 1172) and zero-offset VSP is discussed in Section 5.2 (Figure 9).



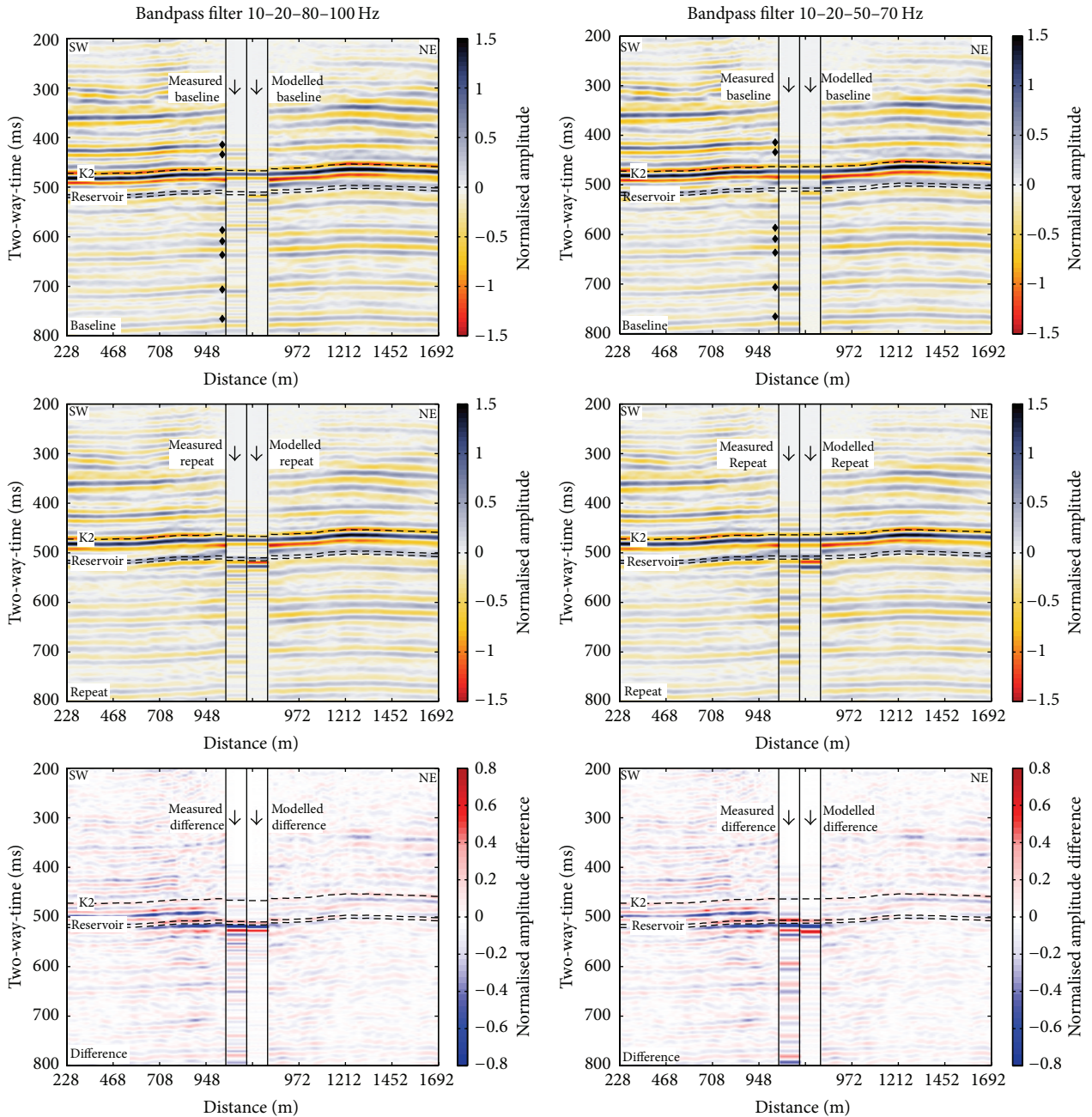


FIGURE 8: Comparison of zero-offset VSP with 3D surface seismic. A detail of the 3D surface seismic inline 1172, which crosses the observation well Ktzi202 (Figure 2) is shown. The traces of the measured and modelled VSP are plotted side by side and inserted at the intersection of inline 1172 with the well. From top to bottom baseline, repeat and difference (repeat minus baseline) of 3D surface seismic and VSP are shown. Consistent phases of 3D surface seismic and zero-offset VSP are marked with diamonds. The VSP data of the left column is bandpass filtered with corner frequencies of 10–20–80–100 Hz; the VSP data of the right column is bandpass filtered with corner frequencies of 10–20–50–70 Hz. The black lines mark the positions of the K2 (upper line), the top, and the bottom of the reservoir (middle and bottom line).

### 5. Discussion

When monitoring CO<sub>2</sub> injection, special attention should be paid to the repeatability of the time-lapse data. There are many factors influencing the time-lapse effects in the zero-offset VSP data in Ketzin. Differences between baseline and repeat can be source related, since for baseline and

repeat measurements sources with different impact energies were used. Furthermore, the source was placed on asphalt close to the well for the baseline measurement, whereas for the repeat it was moved a few meters and activated on gravel, which might reduce the influence of the casing and lead to a stronger attenuation of the signal at higher frequencies in the repeat data (Section 2.1). The age of the

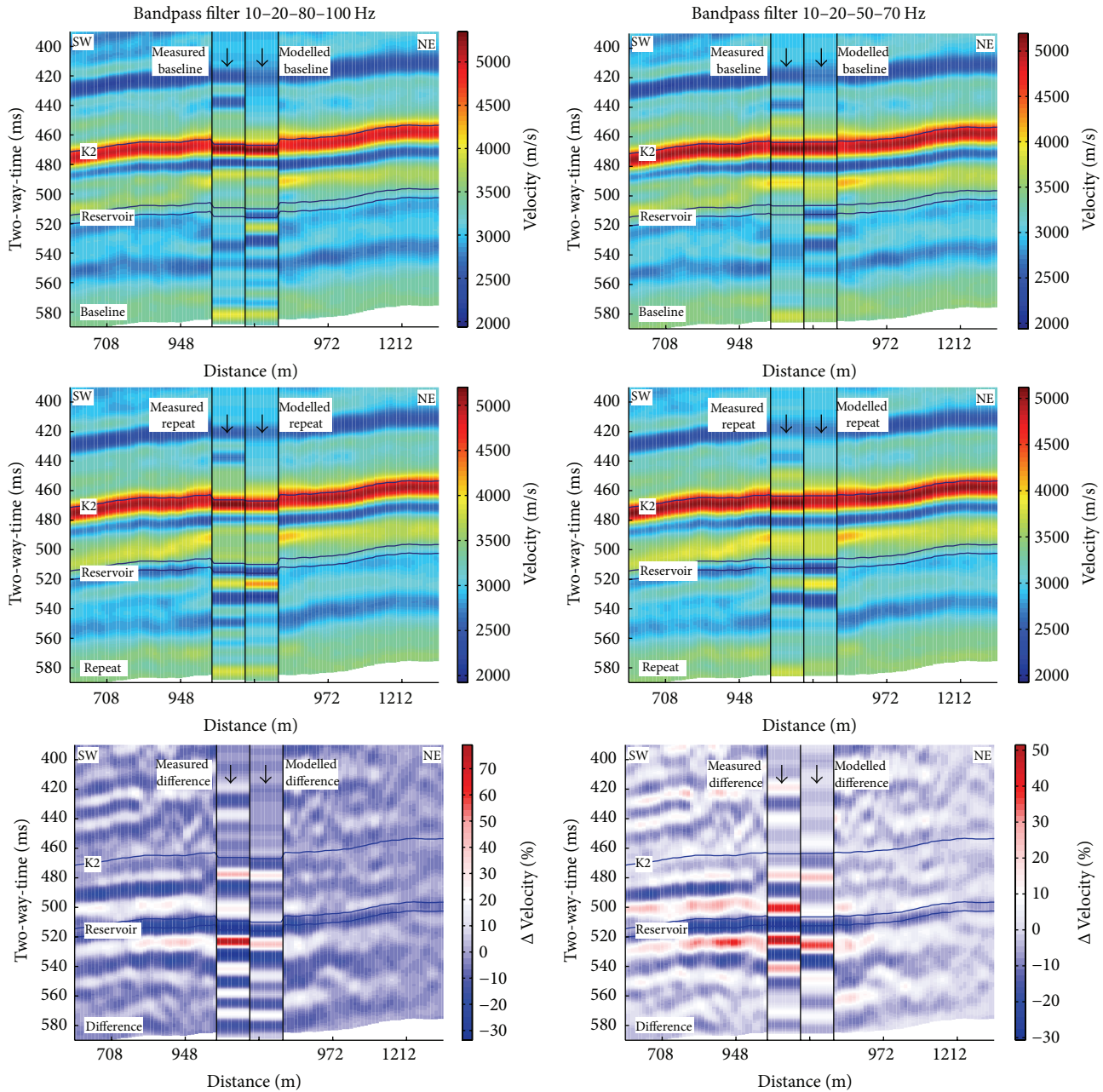


FIGURE 9: Result of the band limited impedance inversion of 3D surface seismic (inline 1172) and zero-offset VSP converted to P-wave velocities. The stacked traces of the zero-offset VSP data (measured and modelled) are plotted side by side and inserted at the intersection of inline 1172 with the well. From top to bottom: baseline, repeat, and difference (repeat minus baseline) in percent of the baseline velocity. The VSP data of the left column is bandpass filtered with corner frequencies of 10–20–80–100 Hz; the VSP data of the right column is bandpass filtered with corner frequencies of 10–20–50–70 Hz. The black lines mark the positions of the K2 (upper line), the top, and bottom of the reservoir (middle and bottom line).

receiver well can have an effect on the repeatability: better seismic bonding to the formation has been observed as a well ages, since drilling mud, rock cuttings, and sloughing that fill the annulus between the casing and the formation tend to solidify [38]. Other parameters to keep in mind are source and receiver positions, receiver coupling, near surface effects (e.g., different weather conditions), and different noise levels. Time-lapse processing should minimise differences in

the data sets, while the actual time-lapse anomaly should be preserved. In this study, the repeat traces are matched to the baseline traces by application of a cross-correlation time-shift (Section 2.3, [30]). In order to increase the correlation between the baseline and repeat surveys a bandpass filter and a Wiener filter are applied (Section 2.4). A parameter to assess the quality of the seismic match is the normalised RMS error (NRMS) [39]. The NRMS ranges from 0% (datasets are

identical) to 200% (datasets are completely anticorrelated, e.g., identical but polarity reversed). The NRMS of the raw data, calculated over the whole trace including the reservoir, is 126%, the application of the bandpass filter reduces it to 112%, and by Wiener filtering it is further improved to 76%.

*5.1. Comparison of Zero-Offset VSP with 3D Surface Seismic.* The processed traces are vertically stacked (median stack) and subsequently duplicated 9 times before displaying. Figure 8 shows from top to bottom baseline, repeat, and difference (repeat minus baseline) of 3D surface seismic and zero-offset VSP. Two different bandpass filters are applied: in order to compare zero-offset VSP baseline and repeat data, a bandpass with corner frequencies of 10–20–80–100 Hz is used (Figure 8, left column). For comparison of the zero-offset VSP with the 3D surface seismic a bandpass with corner frequencies of 10–20–50–70 Hz is applied (Figure 8, right column). The different data sets are normalised to the centre peak of the K2 reflection from the anhydrite layer. Furthermore, the K2 reflections of zero-offset VSP and 3D surface seismic are matched in time. Time-shifts are caused by various statics applied to the 3D surface data like bulk static shifts to compensate for source delay, refraction statics, and residual statics [19]. The black lines in Figure 8 mark the positions of the K2 (upper line) and the top and bottom of the reservoir (middle and bottom line). The K2 is picked within the upper trough of the strong double reflection (trough-peak-trough, [40]). Since the reservoir is not indicated as a clear reflection, it is marked 43 ms after the K2 pick. The time-differences between K2 and reservoir are derived by a well-tie of the sonic log.

When comparing time-lapse zero-offset VSP and 3D surface seismic, one has to bear in mind that the associated repeat measurements were recorded at different times. The 3D surface seismic repeat was recorded in autumn 2009 with 22 kt–25 kt of CO<sub>2</sub> injected, whereas the zero-offset VSP was repeated in February 2011 with 46 kt of CO<sub>2</sub> injected (Table 1).

*(1) Baseline (Figure 8, Top Row).* The dynamic range of the amplitudes of 3D surface seismic, recorded, and modelled zero-offset VSP is comparable. It is possible to identify consistent phases between 3D surface seismic and zero-offset VSP, marked with diamonds in the figure. Contrary to 3D surface seismic and recorded zero-offset VSP, the reservoir is indicated as a reflection (positive amplitude) in the modelled baseline data for both frequency bands. The recorded VSP baseline exhibits weak amplitudes from top of the reservoir to 600 ms two-way-time. This is related to an uncemented part of the single casing string (Figure 3).

*(2) Repeat (Figure 8, Middle Row).* Increased reflectivity, caused by the increased impedance contrast between the caprock and the CO<sub>2</sub> saturated reservoir sandstone, is observed in the zero-offset VSP repeat data. The amplitudes of the high frequency VSP data (left side) show a strong amplitude signature, with ringing extending almost 70 ms below the reservoir. Within the bandpass filtered data (right side) the increased amplitudes are confined to reservoir depth. More details of the structure below the top of the

reservoir are resolved in the zero-offset VSP repeat data than in the 3D surface seismic data. Phases and amplitudes of recorded and modelled repeat are in good agreement besides a slight shift below the reservoir.

*(3) Difference (Figure 8, Bottom Row).* Within the difference sections (repeat minus baseline), a clear amplitude signature at reservoir depth is observed. The signature is influenced by casing reverberations as well as CO<sub>2</sub> injection. The first amplitude sequence (positive-negative-positive) at the top of the reservoir is consistent with 3D surface seismic and modelling data, which indicates a CO<sub>2</sub> influence. The casing reverberations lead to an amplified amplitude of the signature and ringing below the reservoir level. A better confinement of the signature to the reservoir can be achieved by the 10–20–50–70 Hz bandpass filter.

*5.2. Determination of Velocity Changes.* For the quantification of the injected CO<sub>2</sub> volume, the CO<sub>2</sub> saturation is an important reservoir parameter. Based on a petrophysical model it is possible to relate the CO<sub>2</sub> saturation to changes in P-wave velocity [16, 41, 42]. P-wave velocities can be derived from VSP data by calculating differences in direct arrival times [43] or with coda-wave interferometry [44, 45]. Both methods have been tested for the zero-offset VSP data in Ketzin, but they proved susceptible to noise, picking the first arrivals or multiples (Yang, pers. comm.). The band limited impedance inversion produces robust and reliable results and enables direct comparison with 3D surface seismic data.

Figure 9 shows the results of band limited impedance inversion of 3D surface seismic (inline 1172) and zero-offset VSP, converted to P-wave velocities. From top to bottom baseline, repeat and difference (repeat minus baseline) in percent of the baseline velocity are shown. The seismic sections corresponding to this velocity sections are shown in Figure 8.

The general velocity structure is correctly inverted; for example, the P-wave velocity of the K2 is 5500 m/s and the baseline velocity within the reservoir is 3000 m/s (Figure 9, top row). Using the band limited impedance inversion it was not possible to resolve all thin layers evident on the well logs. The K2 reflector is compressed to a single high velocity layer but still accompanied by a low velocity oscillation. The reservoir becomes visible in the repeat data, due to the decreased P-wave velocity. The decrease in velocity is caused by the replacement of brine with CO<sub>2</sub> in the effective pore volume of the reservoir sandstone. Resolving the reservoir by band limited impedance inversion was not possible; the wavefield character is still dominating (Figure 9, middle row). However, it is possible to gain an estimate of the velocity change within the reservoir (Figure 9, bottom row). The modelled data are based on a velocity reduction of 30%; after processing and inversion a velocity reduction of 27% and 22% was found for the high and low frequency data, respectively. The velocity change at the top of the reservoir is 30% for the recorded data (for both bandpass ranges).

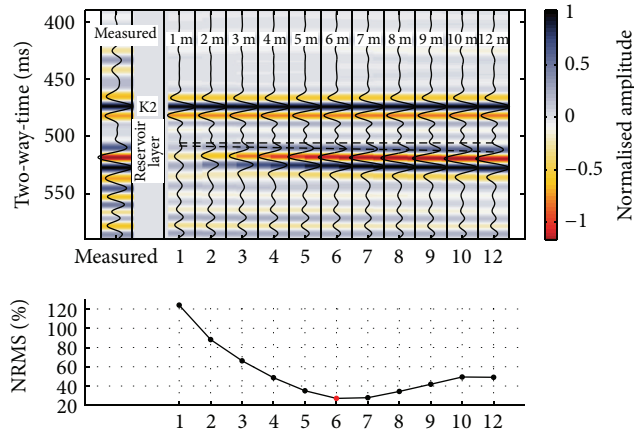


FIGURE 10: Result of wedge modelling for the 10–20–80–100 Hz bandpass filtered data. Top: the corridor-stacked trace of the measured repeat is plotted on the left side. The coloured amplitudes are overlain by the wiggle trace. On the right, the result of wedge modelling is shown, from left to right for 1 m to 12 m reservoir thickness. The top and bottom of the reservoir are plotted as dashed black lines. Bottom: NRMS error between the modelled and measured traces.

The analysis of PNG logging ( $\text{CO}_2$  saturation measurements) performed in March 2011 leads to a mean  $\text{CO}_2$  saturation in the reservoir sandstone close to Ktzi202 of 49% [34]. According to the petrophysical laboratory experiments (see Section 1, [19]), a  $\text{CO}_2$  saturation of 40%–60% would lead to a P-wave velocity reduction ranging from 16% to 21%, which is lower than the velocity reduction of 30% estimated from the VSP data.

A number of reasons can lead to the discrepancy in the velocity contrast measured at laboratory scale and at reservoir scale. (1) The laboratory measurements are based on two core samples which might not entirely represent the heterogeneous sandstone of the reservoir. (2) Seismic wave velocities are frequency dependent, generally the velocity increases with frequency. This effect can lead to a mismatch between the ultrasonic laboratory measurements and the field measurements. (3) The velocity reduction of 30%, inferred from the VSP measurements, cannot be attributed to  $\text{CO}_2$  saturation, only. As for the amplitude difference (Section 5.1), the velocity change is influenced by casing reverberations as well as  $\text{CO}_2$  injection.

**5.3. Estimation of the Vertical Expansion of the  $\text{CO}_2$  Plume from Zero-Offset VSP Data.** When using seismic methods to quantify the injected  $\text{CO}_2$  volume, it is necessary to estimate the plume thickness. Wedge modelling is a traditional approach to link the reflection amplitude of thin layers to the layer thickness [46, 47]. This approach has been used to estimate the vertical expansion of the  $\text{CO}_2$  plume at the Sleipner injection site [48, 49].

At Ketzin, the sandstone layer of the reservoir close to Ktzi202 has a thickness of 8 m. When modelling the VSP experiment it was assumed that the vertical expansion of the  $\text{CO}_2$  plume equals the reservoir layer thickness. A possible alternative scenario would be that the  $\text{CO}_2$  plume migrates along the top of the reservoir, filling it only partially [50]. In order to derive an estimate of the  $\text{CO}_2$  plume thickness based on the zero-offset VSP data, a wedge model study

was performed based on the P-wave, S-wave, and density model shown in Figure 6. The thickness of the reservoir layer, characterised by a 30% P-wave velocity reduction (as determined in Section 5.2), is reduced stepwise from 12 m to 1 m. Figure 10 shows the result of wedge modelling for the 10–20–80–100 Hz bandpass filtered data.

The reservoir is not resolved as separate reflection events and the wavefield is characterised by the interference of reflections from top and bottom of the reservoir (positive-negative-positive). Interference tuning is observed, when the vertical expansion of the  $\text{CO}_2$  saturated layer is reduced in the model. When using the NRMS error as a measure for the similarity between the modelled and recorded repeat traces, the best match is achieved for a plume thickness of 6–7 m within the reservoir sandstone of 8 m thickness. This could reflect results of the PNG logging performed in March 2011. Baumann [34] found a higher  $\text{CO}_2$  saturation of >50% in the upper 4 m of the sandstone layer; in the lower part the saturation is reduced to ~30%.

## 6. Conclusions

Within the framework of CCS exploration, the case study in Ketzin shows that it is possible to identify consistent phases within 3D surface seismic data and zero-offset VSP data. The dynamic range of the amplitudes is comparable for both methods. More details of the structure below the top of the reservoir are resolved in the zero-offset VSP data than in the 3D surface seismic data (Figure 8). Modelled and measured zero-offset VSP data are in good agreement, as well. The time-lapse analysis of zero-offset VSP data evidences  $\text{CO}_2$ -induced amplitude changes (Figure 8, bottom row), but the signature is also influenced by casing reverberations. A better confinement of the signature to the reservoir can be achieved with the application of a 10–20–50–70 Hz bandpass filter (Section 5.1).

The amplitudes of the baseline and repeat zero-offset VSP measurements, after time-lapse processing and bandpass

filtering, are considered to have a sufficient reliability for the deduction of reservoir parameters. It is investigated, whether CO<sub>2</sub>-induced amplitude changes in the monitoring data can be used to derive geometrical and petrophysical parameters governing the migration of CO<sub>2</sub> within the sandstone aquifer, in particular the reduction of P-wave velocity (band limited impedance inversion) and the vertical expansion of the CO<sub>2</sub> plume (wedge modelling). These parameters are needed for the quantification of the injected CO<sub>2</sub> volume.

By performing a band limited impedance inversion it is possible to gain an estimate of the velocity change within the reservoir (Figure 9, bottom row). With PNG logging, a mean CO<sub>2</sub> saturation of 49% is determined, for which petrophysical laboratory experiments would predict P-wave velocity reductions of 16%–21%. The modelled zero-offset VSP data are based on a velocity reduction of 30%; after processing and inversion a velocity reduction of 27% and 22% was found for the high and low frequency data, respectively. Within the recorded data, the inverted velocity reduction at the top of the reservoir is 30%. Processing and inversion are considered reliable, since the velocity reduction of 30%, specified in the seismic-elastic model, is recovered with sufficient accuracy. Nevertheless, the inverted zero-offset VSP velocity reduction should be regarded as an upper bound, since the amplitudes are influenced by casing reverberations as well as CO<sub>2</sub> injection. To take these uncertainties into account when calculating the injected CO<sub>2</sub> volume, the computation of minimum and maximum scenarios could be inevitable.

Figure 10 shows the results of a wedge modelling study. When using the NRMS error as a measure for the similarity between the modelled and recorded repeat traces, the best match is achieved for a plume thickness of 6–7 m within the reservoir sandstone of 8 m. This could reflect the decreasing CO<sub>2</sub> saturation within the reservoir sandstone measured with PNG logging. Wedge modelling can be used to derive the relationship of reflection amplitude to CO<sub>2</sub> layer thickness. For the quantification of the CO<sub>2</sub> volume, a combination of independent ways of obtaining layer thicknesses, like wedge modelling, spectral decomposition, or the analyses of time delays, may improve the understanding of the accuracy of the results.

Zero-offset VSP measurements provided near-well corridor stacks and information about normal incidence reflectivity. It was possible to estimate the thickness of the CO<sub>2</sub> layer and the reduction of P-wave velocity.

Uncemented parts of the casing have a significant effect on the data quality. The analysis of the upper part of the zero-offset VSP in Ketzin was not possible, since the receivers were placed in uncemented multiple casing. In the depth range of the reservoir, casing reverberations influenced the signal and the imaging of the CO<sub>2</sub>. This could be avoided by measuring in properly cemented wells, or by the utilisation of sensors installed behind the casing. The latter also overcomes the need of a lubricator to enter the well. Further analysis could include the estimation of attenuation, an important parameter for the characterisation of properties like saturation, porosity, permeability, and viscosity.

## Conflict of Interests

The authors declare that there is no conflict of interests regarding the publication of this paper.

## Acknowledgments

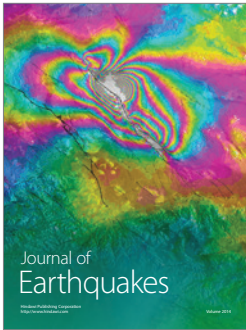
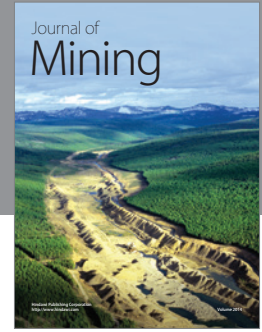
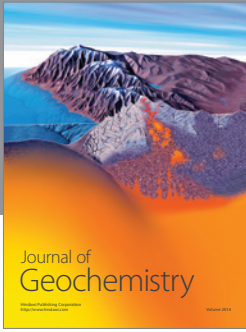
This work was performed in the framework of the European Union Projects CO<sub>2</sub>SINK (no. 502599) and CO<sub>2</sub>ReMoVe (no. 518350) and supported by the Geotechnologien Programme of the German Federal Ministry of Education and Research, BMBF (Project CO<sub>2</sub>MAN, AZ 03G0760A, publication no. GEOTECH-2162), with additional support by the industry partners VNG, Vattenfall, RWE, Statoil, Dillinger Hüttenwerke, Saarstahl, and OMV. The authors would like to acknowledge the contributions and valuable discussions with the Ketzin seismic monitoring group: Monika Ivandic, Alexandra Ivanova, Magdalena Diersch, Christopher Juhlin, Artem Kashubin, Can Yang, and Fengjiao Zhang.

## References

- [1] S. D. Hovorka, T. A. Meckel, and R. H. Treviño, "Monitoring a large-volume injection at Cranfield, Mississippi-Project design and recommendations," *International Journal of Greenhouse Gas Control*, vol. 18, pp. 345–360, 2013.
- [2] S. D. Hovorka, S. M. Benson, C. Doughty et al., "Measuring permanence of CO<sub>2</sub> storage in saline formations: the Frio experiment," *Environmental Geosciences*, vol. 13, no. 2, pp. 105–121, 2006.
- [3] P. Ringrose, A. Mathieson, I. Wright et al., "The in Salah CO<sub>2</sub> storage project: lessons learned and knowledge transfer," *Energy Procedia*, vol. 37, pp. 6226–6236, 2013.
- [4] S. Martens, T. Kempka, A. Liebscher et al., "Europe's longest-operating on-shore CO<sub>2</sub> storage site at Ketzin, Germany: a progress report after three years of injection," *Environmental Earth Sciences*, vol. 67, no. 2, pp. 323–334, 2012.
- [5] K. Kikuta, S. Hongo, D. Tanase, and T. Ohsumi, "Field test of CO<sub>2</sub> injection in Nagaoka, Japan," in *Greenhouse Gas Control Technologies 7*, E. Rubin, D. Keith, C. Gilboy et al., Eds., pp. 1367–1372, Elsevier Science, Oxford, UK, 2005.
- [6] J. Underschlutz, C. Boreham, T. Dance et al., "CO<sub>2</sub> storage in a depleted gas field: an overview of the CO<sub>2</sub>CRC Otway Project and initial results," *International Journal of Greenhouse Gas Control*, vol. 5, no. 4, pp. 922–932, 2011.
- [7] C. Hermanrud, T. Andresen, O. Eiken et al., "Storage of CO<sub>2</sub> in saline aquifers—lessons learned from 10 years of injection into the Utsira Formation in the Sleipner area," *Energy Procedia*, vol. 1, no. 1, pp. 1997–2004, 2009.
- [8] S. Whittaker, B. Rostron, C. Hawkes et al., "A decade of CO<sub>2</sub> injection into depleting oil fields: monitoring and research activities of the IEA GHG Weyburn-Midale CO<sub>2</sub> monitoring and storage project," *Energy Procedia*, vol. 4, pp. 6069–6076, 2011.
- [9] IPCC, *Special Report on Carbon Dioxide Capture and Storage: Prepared by Working Group III of the Intergovernmental Panel on Climate Change*, Cambridge University Press, New York, NY, USA, 2005.
- [10] R. Arts, X. Zhang, A. Verdel et al., "Experiences with a permanently installed seismic monitoring array at the CO<sub>2</sub> storage site

- at Ketzin (Germany)—a status overview,” *Energy Procedia*, vol. 37, pp. 4015–4023, 2013.
- [11] R. Chadwick, D. Noy, R. Arts, and O. Eiken, “Latest time-lapse seismic data from Sleipner yield new insights into CO<sub>2</sub> plume development,” *Energy Procedia*, vol. 1, no. 1, pp. 2103–2110, 2009.
  - [12] D. White, “Seismic characterization and time-lapse imaging during seven years of CO<sub>2</sub> flood in the Weyburn field, Saskatchewan, Canada,” *International Journal of Greenhouse Gas Control*, vol. 16, supplement 1, pp. S78–S94, 2013.
  - [13] J. B. Ajo-Franklin, J. Peterson, J. Doetsch, and T. M. Daley, “High-resolution characterization of a CO<sub>2</sub> plume using crosswell seismic tomography: Cranfield, MS, USA,” *International Journal of Greenhouse Gas Control*, vol. 18, pp. 497–509, 2013.
  - [14] K. Onishi, T. Ueyama, T. Matsuoka et al., “Application of crosswell seismic tomography using difference analysis with data normalization to monitor CO<sub>2</sub> flooding in an aquifer,” *International Journal of Greenhouse Gas Control*, vol. 3, no. 3, pp. 311–321, 2009.
  - [15] M. Urosevic, R. Pevzner, V. Shulakova, A. Kepic, E. Caspari, and S. Sharma, “Seismic monitoring of CO<sub>2</sub> injection into a depleted gas reservoir—Otway Basin Pilot Project, Australia,” *Energy Procedia*, vol. 4, pp. 3550–3557, 2011.
  - [16] T. M. Daley, L. R. Myer, J. E. Peterson, E. L. Majer, and G. M. Hoversten, “Time-lapse crosswell seismic and VSP monitoring of injected CO<sub>2</sub> in a brine aquifer,” *Environmental Geology*, vol. 54, no. 8, pp. 1657–1665, 2008.
  - [17] A. Förster, B. Norden, K. Zinck-Jørgensen et al., “Baseline characterization of the CO<sub>2</sub>SINK geological storage site at Ketzin, Germany,” *Environmental Geosciences*, vol. 13, no. 3, pp. 145–161, 2006.
  - [18] A. Förster, R. Schöner, H. J. Förster et al., “Reservoir characterization of a CO<sub>2</sub> storage aquifer: the Upper Triassic Stuttgart Formation in the Northeast German Basin,” *Marine and Petroleum Geology*, vol. 27, no. 10, pp. 2156–2172, 2010.
  - [19] M. Ivandic, C. Yang, S. Lüth, C. Cosma, and C. Juhlin, “Time-lapse analysis of sparse 3D seismic data from the CO<sub>2</sub> storage pilot site at Ketzin, Germany,” *Journal of Applied Geophysics*, vol. 84, pp. 14–28, 2012.
  - [20] A. Ivanova, A. Kashubin, N. Juhojuntti et al., “Monitoring and volumetric estimation of injected CO<sub>2</sub> using 4D seismic, petrophysical data, core measurements and well logging: a case study at Ketzin, Germany,” *Geophysical Prospecting*, vol. 60, no. 5, pp. 957–973, 2012.
  - [21] B. Norden, A. Förster, D. Vu-Hoang, F. Marcelis, N. Springer, and I. Le Nir, “Lithological and petrophysical core-Log interpretation in CO<sub>2</sub> SINK, the European CO<sub>2</sub> onshore research storage and verification project,” *SPE Reservoir Evaluation & Engineering*, vol. 13, no. 2, pp. 179–192, 2010.
  - [22] C. Yang, C. Juhlin, N. Enescu, C. Cosma, and S. Lüth, “Moving source profile data processing, modelling and comparison with 3D surface seismic data at the CO<sub>2</sub>SINK project site, Ketzin, Germany,” *Near Surface Geophysics*, vol. 8, no. 6, pp. 601–610, 2010.
  - [23] R. Ferguson and G. Margrave, “A simple algorithm for band-limited impedance inversion,” *CREWES Research Report*, vol. 8, pp. 21-1–21-10, 1996.
  - [24] S. H. Kazemeini, C. Yang, C. Juhlin, S. Fomel, and C. Cosma, “Enhancing seismic data resolution using the prestack blueing technique: an example from the Ketzin CO<sub>2</sub> injection site, Germany,” *Geophysics*, vol. 75, no. 6, pp. V101–V110, 2010.
  - [25] T. M. Daley, B. M. Freifeld, J. Ajo-Franklin et al., “Field testing of fiber-optic distributed acoustic sensing (DAS) for subsurface seismic monitoring,” *The Leading Edge*, vol. 32, no. 6, pp. 699–706, 2013.
  - [26] C. Cosma and N. Enescu, “Characterization of fractured rock in the vicinity of tunnels by the swept impact seismic technique,” *International Journal of Rock Mechanics and Mining Sciences*, vol. 38, no. 6, pp. 815–821, 2001.
  - [27] A. Liebscher, S. Martens, F. Möller, and M. Kühn, “Geoscience of carbon dioxide (CO<sub>2</sub>) storage,” in *On-Shore CO<sub>2</sub> Storage in Germany—Experiences Gained from the Ketzin Pilot Site, Brandenburg, the Sole German National CO<sub>2</sub> Storage Project*, J. Gluyas and S. Mathias, Eds., Woodhead Publishing, 2012.
  - [28] P. Keary, M. Brooks, and I. Hill, *An introduction to Geophysical Exploration*, Blackwell Science, 2002.
  - [29] S. Bubshait and D. Lawton, “Zero offset VSP processing for coal reflections,” *CREWES Research Report*, vol. 20, pp. 1–25, 2008.
  - [30] P. Bergmann, C. Yang, S. Lüth, C. Juhlin, and C. Cosma, “Time-lapse processing of 2D seismic profiles with testing of static correction methods at the CO<sub>2</sub> injection site Ketzin (Germany),” *Journal of Applied Geophysics*, vol. 75, no. 1, pp. 124–139, 2011.
  - [31] D. Hampson and L. Mewhort, “Using a vertical seismic profile to investigate a multiple problem in Western Canada,” *Journal of the Canadian Society of Exploration Geophysicists*, vol. 19, no. 1, pp. 16–33, 1983.
  - [32] N. Kaleta, *Time-lapse (4D) seismic investigation of the I3 and TA2 sands, Kilauea Field, Green Canyon Block 6, Gulf of Mexico [Ph.D. thesis]*, The Pennsylvania State University, 2001.
  - [33] B. Wiese, J. Böhner, C. Enachescu, H. Würdemann, and G. Zimmermann, “Hydraulic characterisation of the Stuttgart formation at the pilot test site for CO<sub>2</sub> storage, Ketzin, Germany,” *International Journal of Greenhouse Gas Control*, vol. 4, no. 6, pp. 960–971, 2010.
  - [34] G. Baumann, *Determination of displacement and evaporation/precipitation processes via Pulsed Neutron-Gamma (PNG) monitoring for CO<sub>2</sub> storage operations [Ph.D. thesis]*, Technical University of Berlin, Berlin, Germany, 2013.
  - [35] K. J. Sandmeier, *ReflexW Manual, Version 6.0*, 2011.
  - [36] M. Becquey, M. Lavergne, and C. Willm, “Acoustic impedance logs computed from seismic traces,” *Geophysics*, vol. 44, no. 9, pp. 1485–1501, 1979.
  - [37] G. H. F. Gardner, L. W. Gardner, and A. R. Gregory, “Formation velocity and density—the diagnostic basics for stratigraphic traps,” *Geophysics*, vol. 39, no. 6, pp. 770–780, 1974.
  - [38] B. A. Hardage, *Vertical Seismic Profiling: Principles*, Pergamon, Elsevier Science, 2000.
  - [39] E. Kragh and P. Christie, “Seismic repeatability, normalized rms, and predictability,” *Leading Edge*, vol. 21, no. 7, pp. 640–647, 2002.
  - [40] C. Juhlin, R. Giese, K. Zinck-Jørgensen et al., “3D baseline seismics at Ketzin, Germany: The CO<sub>2</sub> SINK project,” *Geophysics*, vol. 72, no. 5, pp. B121–B132, 2007.
  - [41] S. H. Kazemeini, C. Juhlin, and S. Fomel, “Monitoring CO<sub>2</sub> response on surface seismic data; a rock physics and seismic modeling feasibility study at the CO<sub>2</sub> sequestration site, Ketzin, Germany,” *Journal of Applied Geophysics*, vol. 71, no. 4, pp. 109–124, 2010.
  - [42] T. Vanorio, G. Mavko, S. Vialle, and K. Spratt, “The rock physics basis for 4D seismic monitoring of CO<sub>2</sub> fate: are we there yet?” *Leading Edge (Tulsa, OK)*, vol. 29, no. 2, pp. 156–162, 2010.

- [43] H. Tak, J. Byun, S. J. Seol, and D. G. Yoo, "Zero-offset vertical seismic profiling survey and estimation of gas hydrate concentration from borehole data from the Ulleung Basin, Korea," *Marine and Petroleum Geology*, vol. 47, pp. 204–213, 2013.
- [44] C. Yang, W. Fan, and C. Juhlin, "Coda-wave interferometry analysis of synthetic time-lapse VSP data at CO<sub>2</sub> SINK project site, Ketzin, Germany," in *Proceedings of the EAGE Borehole Geophysics Workshop—Emphasis on 3D VSP*, EarthDoc-47188, Istanbul, Turkey, January 2011.
- [45] R. Zhou, L. Huang, J. T. Rutledge, M. Fehler, T. M. Daley, and E. L. Majer, "Coda-wave interferometry analysis of time-lapse VSP data for monitoring geological carbon sequestration," *International Journal of Greenhouse Gas Control*, vol. 4, no. 4, pp. 679–686, 2010.
- [46] R. S. Kallweit and L. C. Wood, "The limits of resolution of zero-phase wavelets," *Geophysics*, vol. 47, no. 7, pp. 1035–1046, 1982.
- [47] M. Widess, "How thin is a thin bed?" *Geophysics*, vol. 38, no. 6, pp. 1176–1180, 1973.
- [48] R. Arts, O. Eiken, A. Chadwick, P. Zweigel, L. van der Meer, and B. Zinszner, "Monitoring of CO<sub>2</sub> injected at Sleipner using time-lapse seismic data," *Energy*, vol. 29, no. 9-10, pp. 1383–1392, 2004.
- [49] R. Chadwick, R. Arts, and O. Eiken, "4D seismic quantification of a growing CO<sub>2</sub> plume at Sleipner, North Sea," in *Proceedings of the Petroleum Geology Conference Series 6*, pp. 1385–1399, Geological Society, London, UK, 2005.
- [50] U. Lengler, *Einfluss von heterogenen Permeabilitätsfeldern auf die CO<sub>2</sub>-Speicherung in salinen Aquiferen am Beispiel vom Pilotstandort Ketzin [Ph.D. thesis]*, Technische Universität Hamburg, Hamburg, Germany, 2012.



**Hindawi**

Submit your manuscripts at  
<http://www.hindawi.com>

